Geoscience Letters

RESEARCH LETTER

Open Access

Features and mechanisms of sea surface salinity intraseasonal variability in the Northern Bay of Bengal

Rong Cui[1,2], Xuhua Cheng[1,2*], Wei Duan[1,2], Long Jiang[1,2] and Yifei Zhou[1,2]

Abstract

In response to abundant freshwater input from rainfall and river discharge, the northern Bay of Bengal (BoB) is featured by low sea surface salinity (SSS) and strong intraseasonal variability (ISV). This study investigates the characteristic and dynamic mechanisms of SSS ISV in the northern BoB based on satellite observations and the output of Simple Ocean Data Assimilation (SODA). The strong SSS ISV is mainly concentrated near the mouth of the Ganges–Brahmaputra River and along the east coast of India, where the horizontal salinity gradient varies greatly. SSS ISV in the northern BoB is notably in phase with freshwater transport, which peaks from July to November. The contribution of riverine freshwater is significant both geographically and temporally. The SSS budget analysis indicates that the horizontal advection plays a dominant role in SSS ISV. Once currents cross the salinity field, large horizontal advection anomalies become important and favor SSS ISV. Altered SSS patterns can impact water density, potentially influencing the strength and direction of currents. This, in turn, may have cascading effects on local and regional climate patterns.

Keywords Northern Bay of Bengal, Sea surface salinity, Intraseasonal variability, Horizontal advection, Freshwater

Introduction

The Bay of Bengal (BoB) holds a crucial position in understanding the Asian monsoon system (Wang and LinHo 2002) and significantly influences the livelihoods of millions of people dependent on its resources (Balaguru et al. 2012; Krishnan et al. 2011). Salinity plays a key role in these processes. The BoB is characterized by low sea surface salinity (SSS), which is primarily caused by substantial freshwater input through oceanic precipitation and river discharge during the summer monsoon season (Akhil et al. 2014; Papa et al. 2010). The upper layers salinity stratification results in the formation of a barrier layer (Vinayachandran et al. 2001), which hinders the vertical heat and material exchange between the surface mixed layer and interior ocean (Lukas and Lindstrom 1991; Mignot et al. 2007). This, in turn, affects the sea surface temperature, ocean currents, eddies, and upwelling, which ultimately impacts regional climate (Han and McCreary 2001; Howden and Murtugudde 2001; Shenoi et al. 2002; Neetu et al. 2012; Vinayachandran et al. 2012; Sengupta et al. 2008; Yu and McCreary 2004; Guan et al. 2014; Vincent et al. 2012; Rao et al. 2020).

Rao and Sivakumar (2003) identified significant seasonal variations in SSS in the northern BoB. The freshwater flux is the primary factor, and it is mainly driven by river discharge (Sengupta et al. 2006; Han et al. 2001; Benshila et al. 2014; Sandeep et al. 2017). The East India Coastal Current (EICC), a prominent current along the western coast of the BoB, plays a crucial role in transporting seawater, connecting the BoB with the equatorial Indian Ocean and the Arabian Sea (Shankar et al. 1996, 2002; Durand et al. 2009, 2011; Sharma et al. 2010; Shenoi et al. 2005). Horizontal advection driven by EICC helps

*Correspondence:
Xuhua Cheng
xuhuacheng@hhu.edu.cn
[1] Key Laboratory of Marine Hazards Forecasting, Ministry of Natural Resources, Hohai University, No.1 Xikang Road, Nanjing 210098, China
[2] College of Oceanography, Hohai University, Nanjing, China

to maintain the salinity balance within the BoB (Rao and Sivakumar 2003; Wijesekera et al. 2016; Fournier et al. 2017). This balance is closely associated with the surrounding monsoon systems, notably the Indian Summer Monsoon (ISM, Schott and McCreary 2001; Vinayachandran et al. 2013). These monsoon systems are remotely influenced by global coupled modes of variability such as the Indian Ocean Dipole (IOD) and El Niño-Southern Oscillation (ENSO, Vinayachandran and Nanjundiah 2009; Subrahmanyam et al. 2018). They tend to establish teleconnections with salinity in the BoB through rainfall and river runoff (Akhil et al. 2020; Chaitanya et al. 2015; Pant et al. 2015). As a result, salinity exhibits strong interannual variability in autumn. Previous studies on seasonal and interannual variations have highlighted the importance of freshwater, particularly river runoff, in salinity transport (Wu et al. 2007; Seo et al. 2009).

In the past few decades, the scarcity of available field measurements has limited comprehensive studies on SSS variations and related processes (Webster et al. 2002; Vinayachandran and Kurian 2007; Parampil et al. 2010). However, advancements in models and observations have enabled investigations into the ISV of SSS in the northern BoB (Trott et al. 2019; Grunseich et al. 2013). Li et al. (2015) and Zhu et al. (2020) explored the ISV using satellite observations and models in the equatorial region. They revealed that in most areas of the equatorial Indian Ocean, ocean dynamic processes driven by wind stress are the primary drivers, predominantly influencing SSS through horizontal advection, with precipitation playing a secondary role. Only in certain regions of the western Pacific and western Indian Ocean does precipitation contribute significantly to the SSS variations (Li et al. 2015). In the BoB, horizontal advection dominates, and the notable intraseasonal SSS variations are observed in the northern BoB (Li et al. 2017a), especially during the southwest monsoon period (Vinayachandran et al. 2002; Subrahmanyam et al. 2018). The BoB receives approximately 1.5×10^{12} m^3 of freshwater from river runoff annually (Sengupta et al. 2006), with two thirds of the freshwater input occurring from June to September, predominantly in the northern BoB. Madden–Julian Oscillation (MJO) and the Monsoon Intra-Seasonal Oscillation (MISO) are two important atmospheric phenomena that can affect rainfall patterns (Madden and Julian 1971, 1972; Li et al. 2003, 2017a, 2017b), freshwater fluxes and ocean currents thereby potentially impacting the fluctuations of SSS (Schott et al. 2009; Grunseich et al. 2011; Kikuchi and Wang 2009). Considering this, it raises the question whether terrestrial runoff influences the ISV of SSS in the northern BoB.

Despite the existing understanding of the mechanisms driving intraseasonal variations, further efforts are needed to elucidate the role of horizontal advection in modulating the intraseasonal salinity changes. In this paper, we aim to investigate the SSS ISV in the northern BoB (98–100° E, 15° N–25° N, Fig. 2) using high-resolution satellite data and ocean reanalysis products. The remainder of this paper is organized as follows. Section "Data and methods" describes the data and methods used, while section "Results" presents the results. We focus on the period from July to November, which corresponds to the peak freshwater input from rivers and precipitation. Finally, section "Conclusions" summarizes the main conclusions, providing insights into the potential impacts of climate change in the region.

Data and methods

Data

The SMAP SSS data version 4.3 (gridded level-3 dataset) provided by NASA/Jet Propulsion Laboratory (JPL), is used to reveal the features of SSS in the northern BoB. SMAP was launched on January 31, 2015, with the capability to provide global coverage approximately every 3 days, an accurate orbit repetition period of 8 days, and a spatial resolution of 0.25°. The daily SSS data is expertly averaged over 8 days from April 2015 to the present. In comparison to earlier salinity-detectable satellites Aquarius and SMOS, SMAP is capable of inverting the SSS with higher accuracy and boasts a higher horizontal and temporal resolution, as well as a scanning swath of approximately 1000 km (Bao et al. 2019; Tang et al. 2017). The SMAP provides a new and innovative way to study ISV of SSS in the northern BoB (Fournier et al. 2017; Vinogradova, et al. 2019).

To explore the mechanism of the ISV of SSS in the northern BoB, the SSS, sea surface current, mixed layer depth, precipitation, evaporation and river runoff from Simple Ocean Data Assimilation (SODA) are employed in this study. The SODA 3.15.2 is an ensemble reanalysis that has distinct forcings provided by differing atmospheric reanalyses (Carton et al. 2018). The products have an 0.25°×0.25° grid spatial resolution, a temporal resolution of 5 days, and 50 vertical levels.

Methods

Salinity budget equation

The variation of SSS is controlled by evaporation, precipitation, river runoff, horizontal and vertical advection, entrainment and mixing processes. To illustrate the effects of different processes on the evolution of surface salinity, neglecting horizontal diffusion, the salinity budget equation (Rao and Sivakumar 2003; Nyadjro et al. 2012) can be written as

$$\frac{\partial \mathrm{S}}{\partial \mathrm{t}} = -\left(u\frac{\partial \mathrm{S}}{\partial \mathrm{x}} + v\frac{\partial \mathrm{S}}{\partial \mathrm{y}}\right) - \frac{\mathrm{S(P-E+R)}}{\mathrm{h}} - \mathrm{w_e}\frac{S_m - \mathrm{S_{-h}}}{\mathrm{h}} + \mathrm{Residual} \tag{1}$$

where, S is the SSS; P and E are the precipitation and evaporation, respectively; R is the river runoff; h represents the mixed layer depth; u and v represent the zonal and meridional velocity at the sea surface. Due to the shallow mixed layer, the difference between the surface current velocity and the average current velocity of the mixed layer is not significant (Narvekar and Kumar 2006). So, u and v are used to replace the averaged current velocity of the mixed layer for the research region; w_e represents the velocity crossing the bottom of mixed layer, it can be estimated by $w_e = (h_{n+1} - h_{n-1})/(d_t * 2) + w_h$, h_{n+1} are extracted the depth of the mixed layer for the day+1 from a three-dimensional array 'h' at specific indices (i, j); h_{n-1} are extracted the depth of the mixed layer for the day-1; dt represents the time step; w_h epresents the vertical entrainment velocity at the base of the mixed layer, and it is determined using the continuity equation: $w_h = h(\frac{u_{n+1}-u_{n-1}}{2\Delta x} + \frac{v_{n+1}-v_{n-1}}{2\Delta y})$; S_m represents the average salinity of mixed layer and S_{-h} represents the salinity of the bottom of mixed layer. The term on the left-hand side of the equation is the temporal variation of SSS. The first term on the right is the horizontal advection, which represents the transport of salinity by the ocean current. The second term gives the contribution due to freshwater flux, which represents the combined effect of evaporation, precipitation and river runoff. The positive freshwater flux indicates a decrease of SSS, and vice versa. The third term is the vertical entrainment, which represents the transport of the salinity through the bottom of the mixed layer. Compared to the former two terms, the values of third term are quite small (Zhang et al. 2009). Residual denotes the diffusion and mixing processes.

The anomalous advection

To further analyze the role of advection on the SSS variations, it is decomposed by the following process. We substitute $S = \overline{S} + S'$, $u = \overline{u} + u'$ and $v = \overline{v} + v'$ into the advection term and then get that:

$$\begin{aligned} -\left(u\frac{\partial S}{\partial x} + v\frac{\partial S}{\partial y}\right) &= -(\overline{u} + u')\frac{\partial(\overline{S} + S')}{\partial t} - (\overline{v} + v')\frac{\partial(\overline{S} + S')}{\partial t} \\ &= -\left(\overline{u}\frac{\partial \overline{S}}{\partial x} + \overline{v}\frac{\partial \overline{S}}{\partial y}\right) - \left(u'\frac{\partial \overline{S}}{\partial x} + v'\frac{\partial \overline{S}}{\partial y}\right) - \left(\overline{u}\frac{\partial S'}{\partial x} + \overline{v}\frac{\partial S'}{\partial y}\right) - \left(u'\frac{\partial S'}{\partial x} + v'\frac{\partial S'}{\partial y}\right) \end{aligned} \tag{2}$$

where the $\overline{S}$, $\overline{u}$ and $\overline{v}$ are obtained by applying a 60-day of low-pass filter. It has variabilities greater than 60 days, which is the sum of the seasonal cycle, climatological annual-mean value, and interannual variations. Similarly,S', u' and v' are acquired using 30–60-day band-pass filter. The intraseasonal signal and the relatively low frequency signal can be separated by the scale decomposition. The left terms of Eq. (2) can be similarly decomposed into the mean state (low-frequency part) and the disturbed state (intraseasonal part):

$$-\left(u\frac{\partial S}{\partial x} + v\frac{\partial S}{\partial y}\right) = -\overline{\left(u\frac{\partial S}{\partial x} + v\frac{\partial S}{\partial y}\right)} - \left(u\frac{\partial S}{\partial x} + v\frac{\partial S}{\partial y}\right)' \tag{3}$$

While,

$$-\overline{\left(u\frac{\partial S}{\partial x} + v\frac{\partial S}{\partial y}\right)} = -\left(\overline{u}\frac{\partial \overline{S}}{\partial x} + \overline{v}\frac{\partial \overline{S}}{\partial y}\right) - \overline{\left(u'\frac{\partial S'}{\partial x} + v'\frac{\partial S\prime}{\partial y}\right)} \tag{4}$$

Thus,

$$\begin{aligned} -\left(u\frac{\partial S}{\partial x} + v\frac{\partial S}{\partial y}\right)' &= -\left(u'\frac{\partial \overline{S}}{\partial x} + v'\frac{\partial \overline{S}}{\partial y}\right) - \left(\overline{u}\frac{\partial S'}{\partial x} + \overline{v}\frac{\partial S'}{\partial y}\right) \\ &\quad - \left(u'\frac{\partial S'}{\partial x} + v'\frac{\partial S'}{\partial y}\right) + \overline{\left(u'\frac{\partial S'}{\partial x} + v'\frac{\partial S'}{\partial y}\right)} + \mathrm{R1} \end{aligned} \tag{5}$$

Based on the above steps, we decompose the intraseasonal advection into three terms. The left term of the Eq. (5) is the anomalous advection (ADV). The first term on the right side of the equation is the anomalous advection caused by the anomalous current advecting the mean salinity (ADV1). The second term on the right is the anomalous advection caused by the mean current advecting the anomalous salinity (ADV2). The fourth term (ADV4) is the mean state of the third term (ADV3), which is caused by anomalous current advecting the anomalous salinity. $R1$ is the non-linear residual term, which is small and can be ignored.

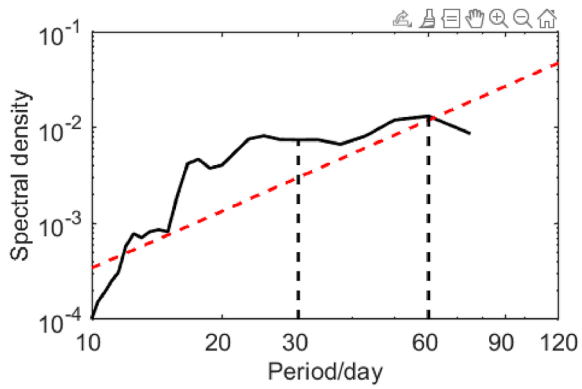

Fig. 1 Power spectra for SMAP sea surface salinity averaged within 98°–100° E, 15° N–25° N. The dashed red curve indicates 95% confidence level

Results

Spatial and temporal distribution of SSS variability

Power spectrum analysis is employed to capture the elusive nature of intraseasonal oscillations (ISOs). The SSS in the northern BoB exhibits prominent high-frequency features, with peaks at 15–60-day (Fig. 1). Because the 15 days is the period for the spring-neap tidal oscillation, we mainly focus on the 30–60-day variability, a range of ISO periods.

The standard deviation (STD) of SSS anomalies (SSSA) for SMAP and SODA is shown in Fig. 2. The SSS ISV exhibits distinct seasonal variations, which is strong during summer and autumn. The SSS ISV also shows remarkable spatial difference. Larger values are primarily located at the northern tip and western coast of the Bay (Fig. 2b, c). The STD of SSS gradient anomalies (Fig. 3) also exhibits significant spatio-temporal variability, in agreement with the SSS ISV (Fig. 2). It indicates that SSS ISV is likely linked to the horizontal salinity gradient. The similar pattern between SSS anomalies and the SSS gradient anomalies indicates that ADV2 and ADV3 in Eq. (5) have considerable contribution to SSS ISV, which will be discussed in section "Mechanism of ISV of sea surface salinity in the northern Bay of Bengal". The STD of SSS and SSS gradient anomalies in SODA show similar pattern to that of SMAP observations, indicating that SODA reproduces the ISV of SSS in the BoB quite well.

Three regions (the black box marked in Fig. 2c) are chosen as typical spots to exhibit the temporal evolution of SSS anomalies. Region A is near the Gange–Brahmaputra River mouth, which is more heavily influenced by freshwater. Region B is along the east coast of India, receiving impact from coastal currents. Region C is far away from continental boundaries and river runoff. In Region A, the SSS reaches its minimum during July–September, due to the influx of freshwater from rainfall and runoff that begins in June and reaches its peak in August–September. The minimum SSS in Regions B and C occurs later than Region A (Fig. 4).

It is also noteworthy that strong SSS ISV in three regions is phase locked to low-salinity period (Figs. 4 and 5). The river runoff peaks during July–October and also exhibit significant ISV (Fig. 6). The observed phase-locked feature suggests a strong influence of MJO and MISO on the regional SSS dynamics. MJO and MISO

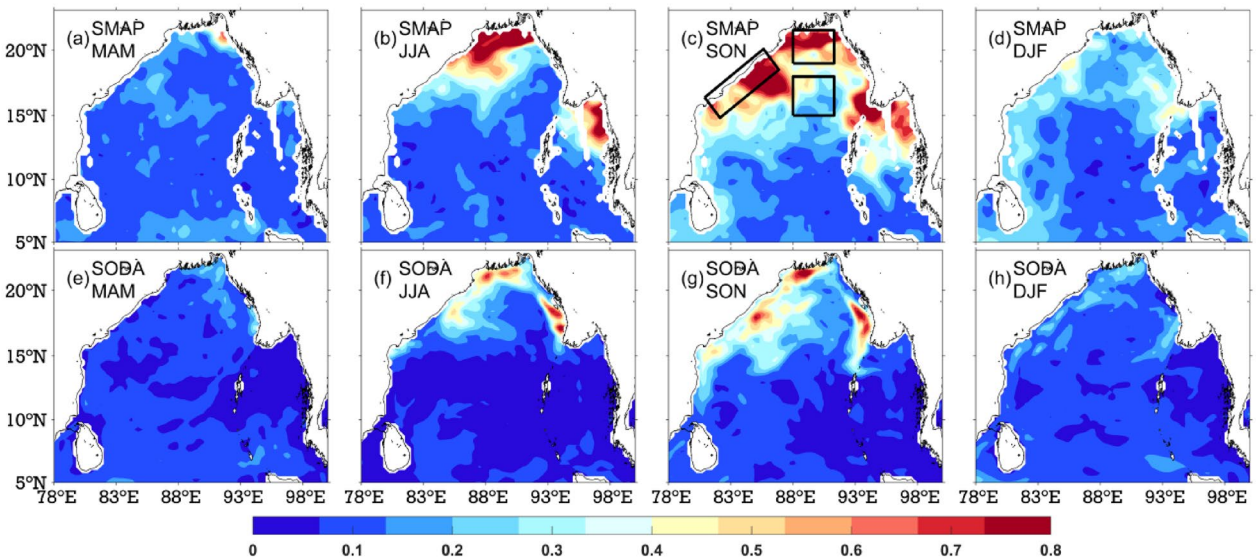

Fig. 2 The upper panel shows the standard deviation (STD) of the 30–60-day filtered SSS anomalies during different seasons from SMAP over 2016–2020. The bottom panel is same as the upper panel but from SODA over 2016–2020 (unit: psu)

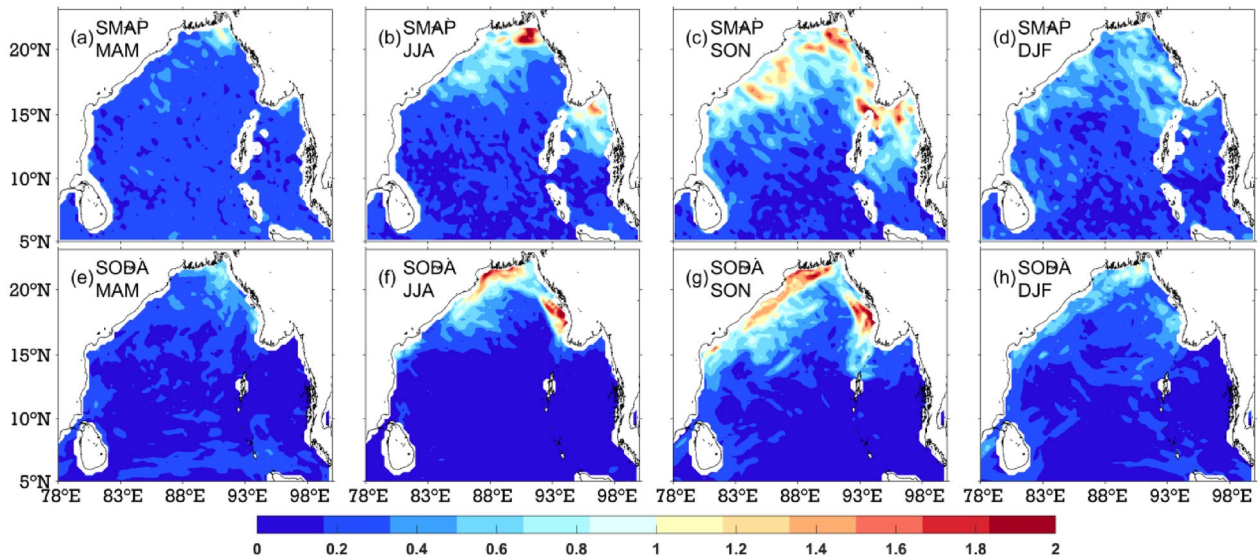

Fig. 3 The upper panel shows the STD of the 30–60-day filtered SSS gradient anomalies during different seasons from SMAP over 2016–2020. The bottom panel is same as the upper panel but from SODA over 2016–2020 (unit: 10^{-2} psu/km)

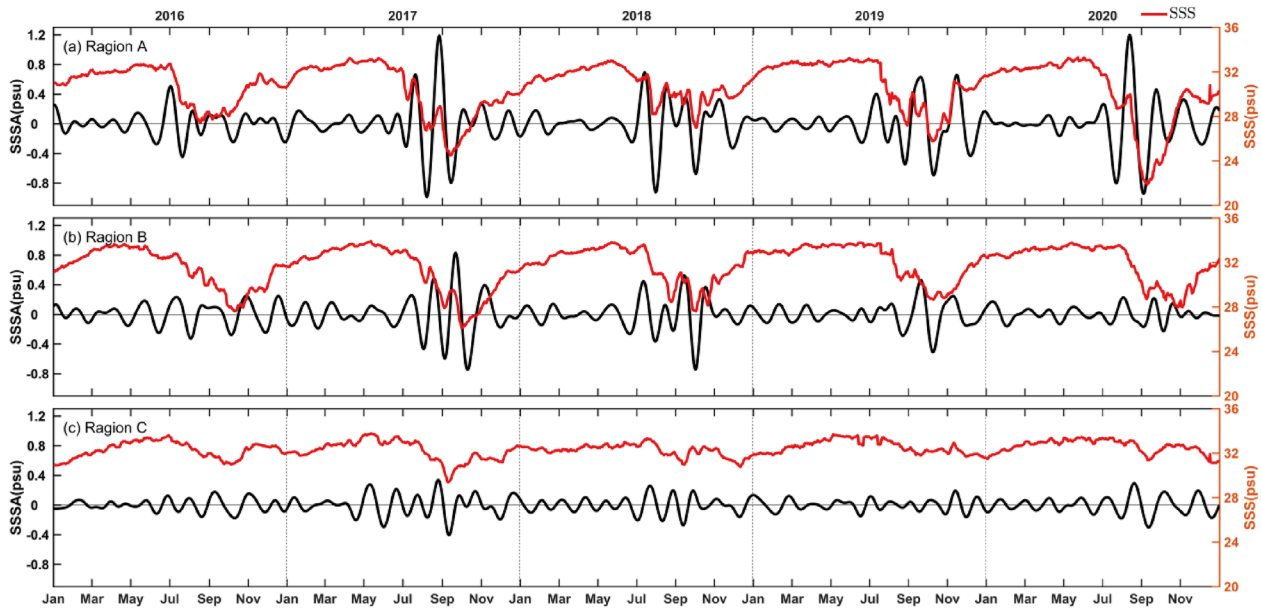

Fig. 4 Time series of 30–60-day filtered daily SMAP SSSA (black, psu) and SMAP SSS (red, psu) for **a** Region A (88°–92° E, 19°–21° N), **b** Region B (within two hundred kilometers of the eastern coast of Indian), and **c** Region C (88°–92° E, 15°–18° N) during 2016–2020, respectively

actively promote convection and heavy rainfall during their active phases. In the BoB, the active phases of MJO and MISO often occur during the summer months, typically from June to September. This period represents a period of increased atmospheric instability and convective activity at intraseasonal timescale. The enhanced convection and increased rainfall during the active phase lead to a pattern of low-salinity conditions, impacting the SSS (Fujinami et al. 2011; Grunseich et al. 2011). Year-to-year differences are evident in Figs. 4, 5, 6. Specifically, the years 2016 and 2018 exhibit stronger ISV in river runoff, corresponding to stronger SSS ISV. Moreover, the SSS ISV in Region C is weaker than that of Regions A and B, which is attributed to the absence of direct influence

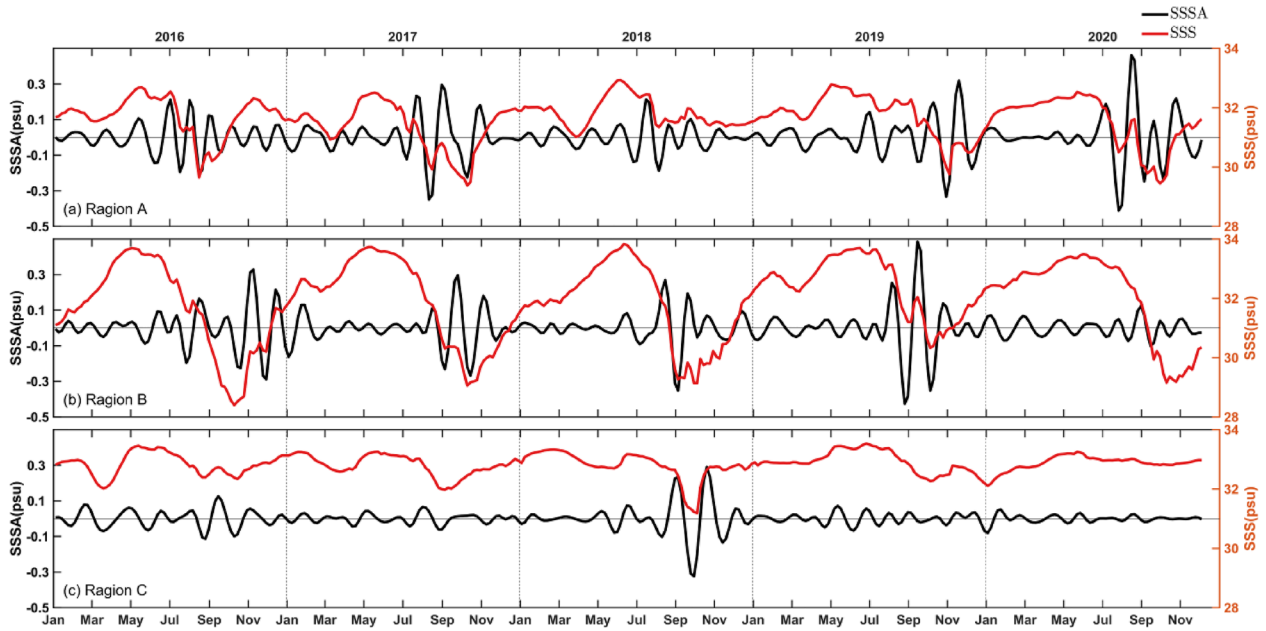

Fig. 5 Time series of 30–60-day filtered daily SODA SSSA (black, psu) and SODA SSS (red, psu) for **a** Region A, **b** Region B, and **c** Region C during 2016–2020, respectively

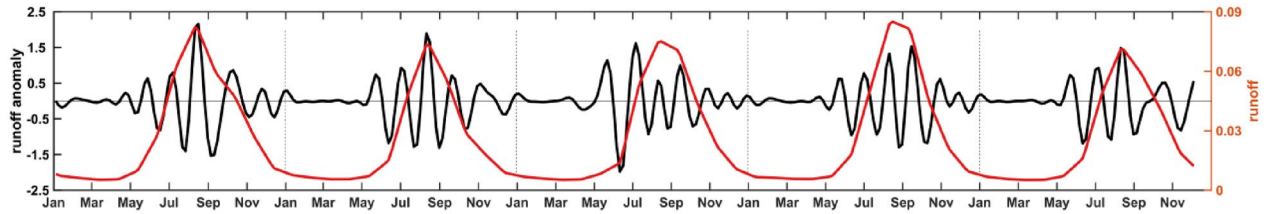

Fig. 6 Time series of 30–60-day filtered daily mass flux of river runoff entering ocean (black, $\times 10^{-3}$(kg/m^3) $*$ (m/s)) and daily mass flux of river runoff (red, (kg/m^3) $*$ (m/s)) for the nBoB from SODA during 2016–2020

from river runoff. The temporal variability of SSSA and SSS is well represented at all locations in SODA, except that their amplitude is slightly weaker than that of SMAP (Figs. 4 and 5). Therefore, the SODA output can be used to diagnose the mechanism of SSS ISV.

Mechanism of ISV of sea surface salinity in the northern Bay of Bengal

The study utilizes the salinity budget equation to diagnose the main contributors to SSS ISV. The temporal evolution in regions A, B, and C displays unique patterns primarily influenced by river runoff, the EICC, and mesoscale eddies. Different time periods exhibit distinct dynamics, emphasizing the varied roles these factors play in shaping SSS ISV in the northern BoB.

Contribution of horizontal advection of salinity to SSS ISV

Figure 7 shows the temporal evolution of various tendency terms of Eq. (1) in three regions. The magnitude of the horizontal advection is much greater than the freshwater flux and vertical entrainment. The horizontal advection is largely consistent with salinity changes. Local rainfall does play a role in freshwater flux, but its impact is largely confined to short time scales, has less impacts on SSS on intraseasonal scales. Consistent with the year-to-year differences in river runoff ISV and SSS ISV, the advection anomalies were also larger in 2016 and 2018, especially in Region B and Region C. The horizontal advection dominates the SSS ISV.

The large amplitudes of SSSA and ADV in Region A from June to November are linked to the supply of

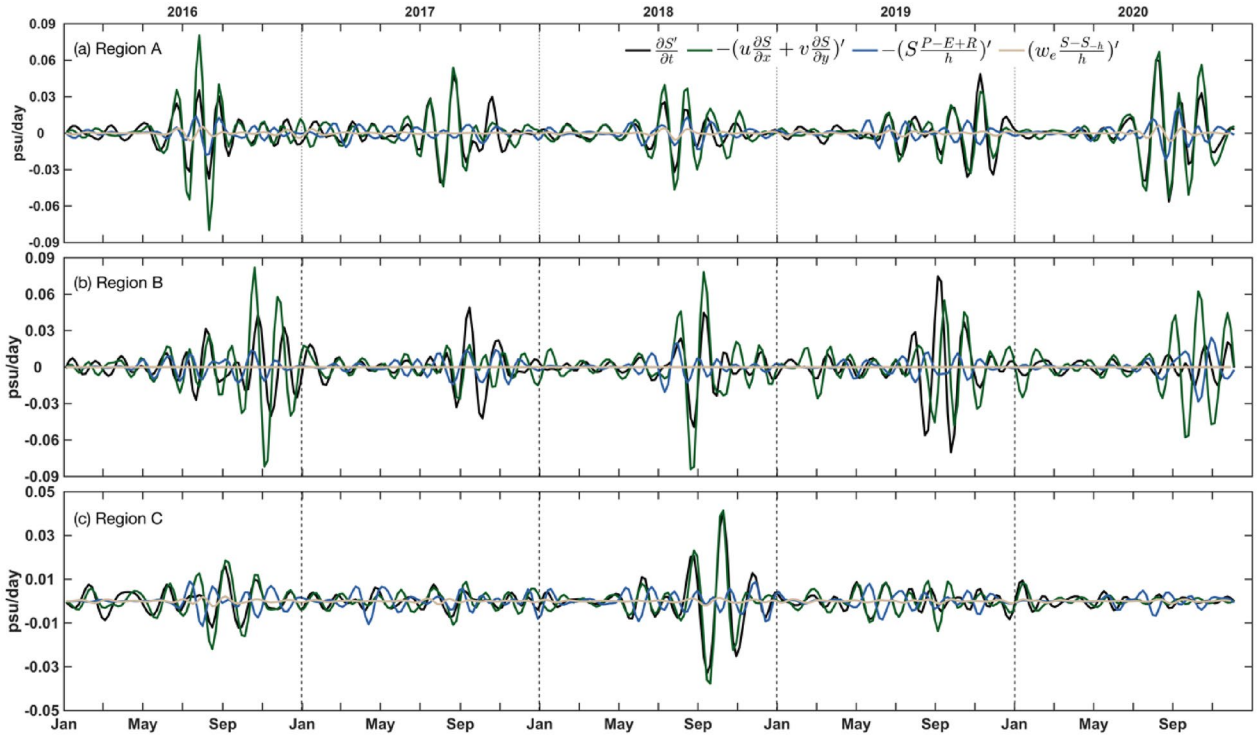

Fig. 7 Time series of 30–60-day filtered salinity budget terms (unit: psu/day) for **a** Region A, **b** Region B, and **c** Region C during 2016–2020 from SODA data, respectively

freshwater from the river runoff during this period (Fig. 6). Freshwater appears to maintain a certain level of balance mainly through three considerable ways, namely atmospheric and continental freshwater flux (precipitation, evaporation, and river runoff), horizontal advection, and vertical processes such as entrainment, vertical mixing, and vertical advection (Eq. (1)). Note that freshwater enters into Region A generally in a near-surface layer, and is transported southward by currents and eddies. As the freshwater is advected by the currents, SSSA and salinity gradients turns larger and stronger. Consequently, the effect of horizontal advection dominates the SSS ISV. This process occurs successively in Region A and Region B because of the pathway of the freshwater.

In Region B, the high values appear in August–November, with peaks that slightly lag behind those in Region A. The direction and magnitude of EICC from Region A to Region B have a profound and indelible impact on the salinity exchange between the two regions, and even on the inflow and outflow of salinity in the whole BoB (Durand et al. 2009). The peak in Region C occurs at a time that is in close proximity to that of Region A, which may be attributed to the influence of Region A. A more detailed analysis of the anomalous horizontal advection will be addressed in the subsequent section.

The role of mean salinity advected by anomalous current

To better understand the impact of various abnormal advection processes on the SSS ISV, the time series of all terms of horizontal advection anomalies for three regions are shown in Fig. 8. The results suggest that ADV1 and ADV2 have the largest magnitudes in all regions. The large amplitudes of them in Region A are primarily concentrated during July–November while that in Region B is during August–December, which is in line with the variations of SSS. The ADV1 and ADV2 terms are two principal contributors to the SSS ISV. Variations in local salinity are a consequence of currents transporting fresher water into and out of the region, with the anomalous currents being of particular importance.

We chose two typical periods to further understand the roles of the anomalous current on anomalous advection. During period I, which is from October 5 to November 19, 2016, the contribution of intraseasonal variations of EICC is explored (Fig. 9, the periods I marked by the first purple shadow). Relatively less freshwater enters the Bay during this period (Fig. 6), so the salinity gradient in Region A was smaller and the salinity transport by the anomalous current was weaker (Fig. 9a). In Region B, the EICC was fully developed, so that the mean salinity transport by the anomalous EICC was strong. Although

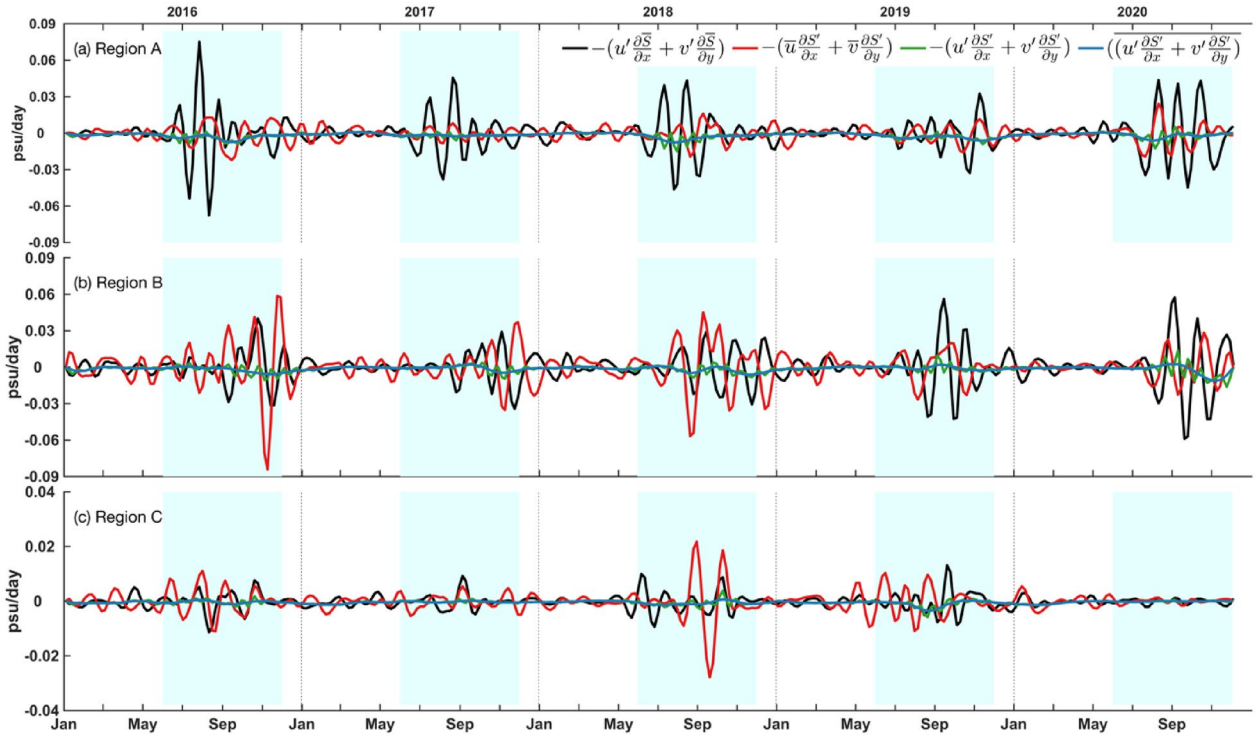

Fig. 8 Time series of ADV1 (black, psu/day), ADV2 (red, psu/day), ADV3 (green, psu/day), and ADV4 (blue, psu/day) for **a** Region A, **b** Region B, and **c** Region C during 2016–2020 from SODA data, respectively

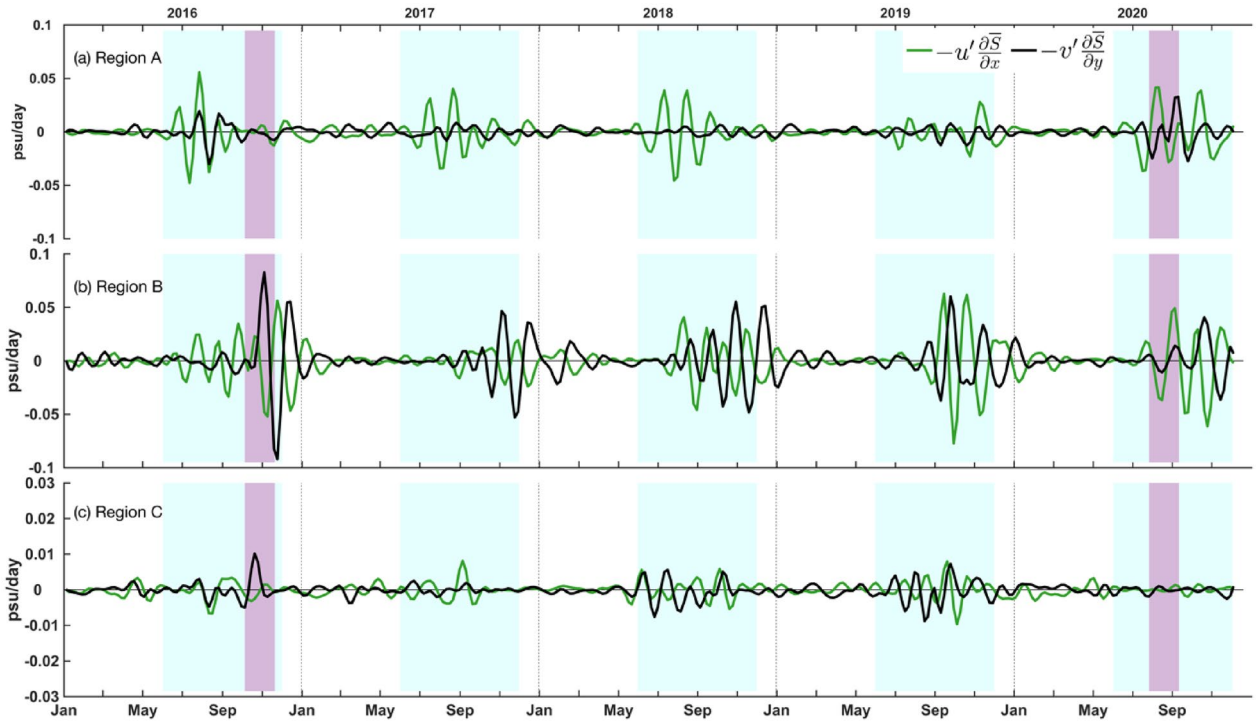

Fig. 9 Time series of mean salinity advected by zonal current anomalies (green, psu/day) and meridional current anomalies (black, psu/day) for **a** Region A, **b** Region B, and **c** Region C during 2016–2020 from SODA data, respectively

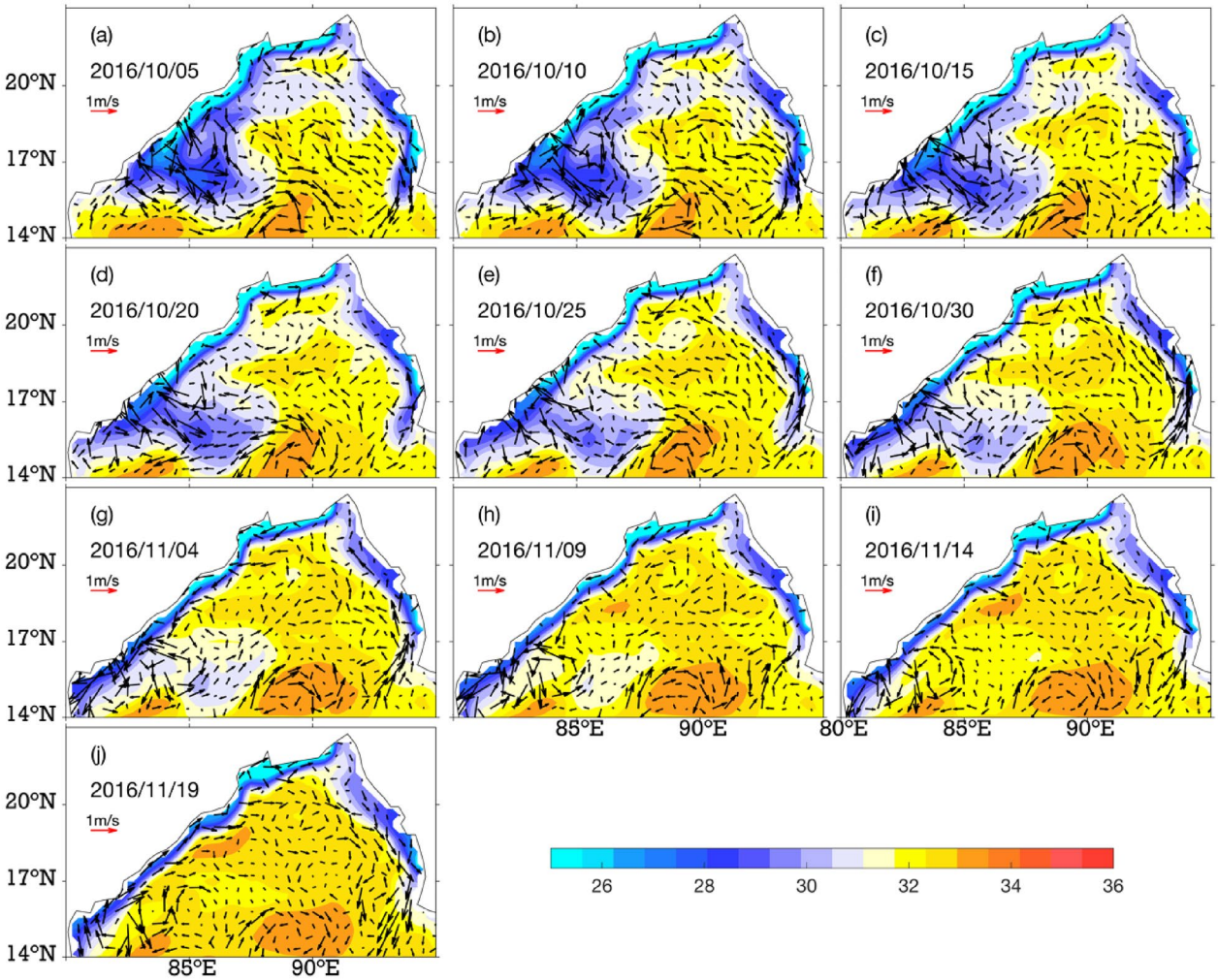

Fig. 10 The maps of mean state SSS (unit: psu) and 30–60-day surface current anomaly (arrows, unit: m/s) from SODA data during the period I

some of these are balanced by salinity transport by zonal current anomalies associated with eddy activities, the meridional salinity transport anomaly is always stronger. So, the variations of salinity in Region B are consistent with EICC anomalies (Figs. 9b and 10).

During period II, which is from July 27 to September 10, 2020 (Fig. 9, the periods II marked by the second purple shadow), a large influx of freshwater accumulates at the surface of Region A, creating a strong salinity gradient (Figs. 6 and 11). The meridional current anomaly and the zonal current anomaly across the salinity front carrying away the local salinity signals (Fig. 9a). When the mean salinity advected by zonal current anomaly (a positive value) surpasses the meridional current anomaly (a negative value) (Fig. 11b, c), resulting in a positive ADV1 there (Fig. 8a). When the mean salinity advected by meridional current anomaly (a positive value) surpasses the zonal current anomaly (a negative value) (Fig. 11j), resulting in a positive ADV1 there (Fig. 8a). Region B is primarily influenced by the freshwater transport from Region A. The anomalous current flow from Region A to Region B, leading to salinity decrease in Region B.

The role of SSS anomalies advected by mean current

Figure 12 shows the time series of the SSS anomalies advected by the mean meridional current and zonal current for SODA in the three regions. To further analyze the transport of salinity anomalies, we examine the

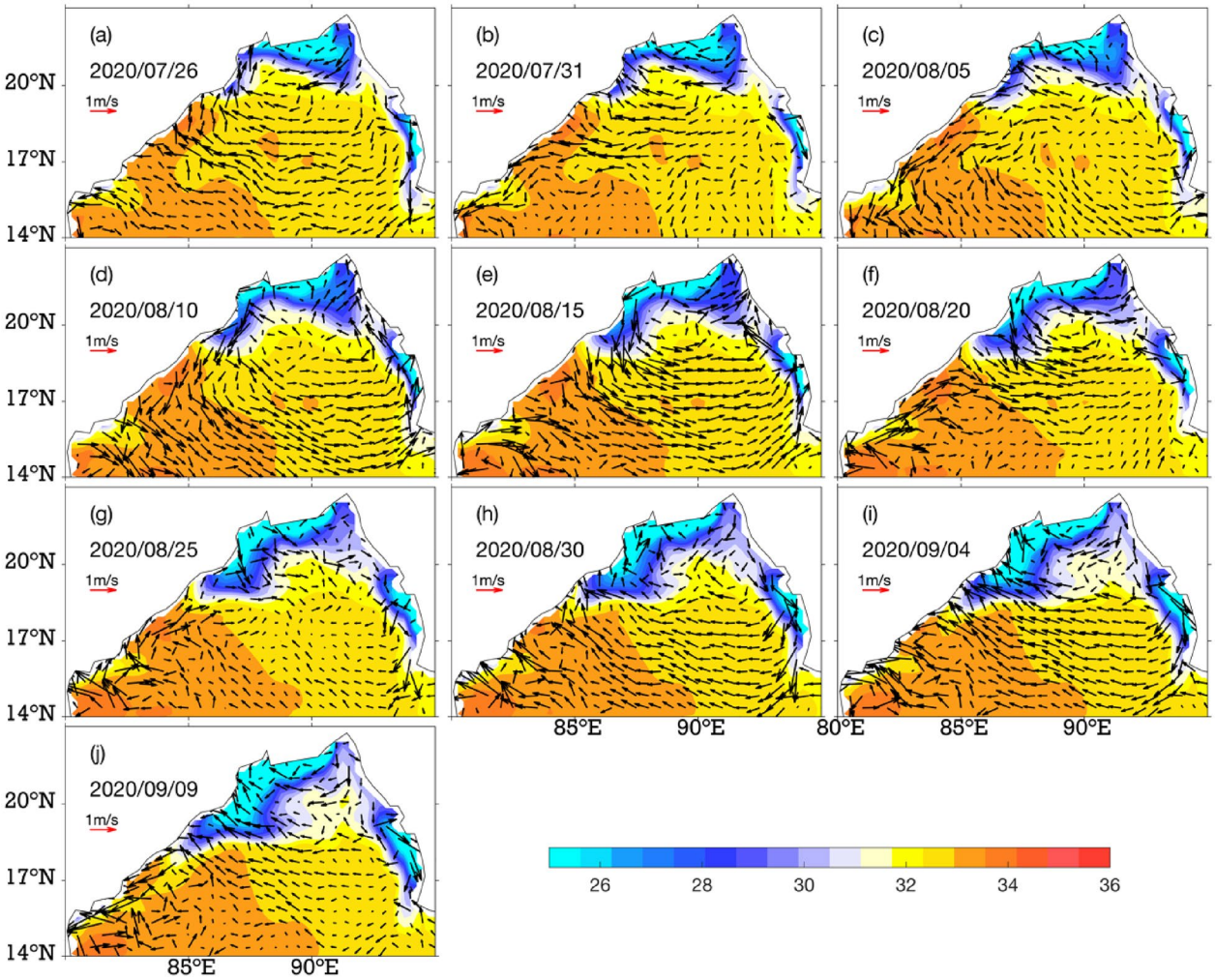

Fig. 11 The maps of mean state SSS (unit: psu) and 30–60-day surface current anomaly (arrows, unit: m/s) from SODA data during the period II

background current field during periods I and II, which were shown in Figs. 13 and 14. During period I, there is a cyclonic eddy in Region A. The effect of meridional and zonal advection is opposite. The amplitudes of both are small due to the small salinity anomaly (Fig. 12a). A southward flow (EICC) from Region A to Region B was observed, which produced a negative anomalous meridional advection when it passes over a negative salinity anomaly in its pathway (Fig. 13). Simultaneously, a strong westward current at 18° N, which is a zonal component of the cyclonic eddy in Region B, generates a positive zonal advection anomaly when there is a negative salinity anomaly along the coast. The transport of salinity anomalies by the meridional and zonal currents is always opposite in this region (Fig. 13b). The transport of salinity anomalies by the meridional current acts to counteract that by the zonal current in Region B. The salinity gradient anomalies in Region C are too small to be analyzed in detail in this study. This is mainly due to Region C being far from freshwater and its pathway.

During period II, positive and negative salinity anomalies coexist in region A. Sometimes the zonal and meridional current is associated with mesoscale eddies. In Fig. 14d and e, the cyclonic eddy tends to transport the positive SSS anomalies westward and southward, out of Region A. These SSS anomaly signals thus flow into Region B and Region C.

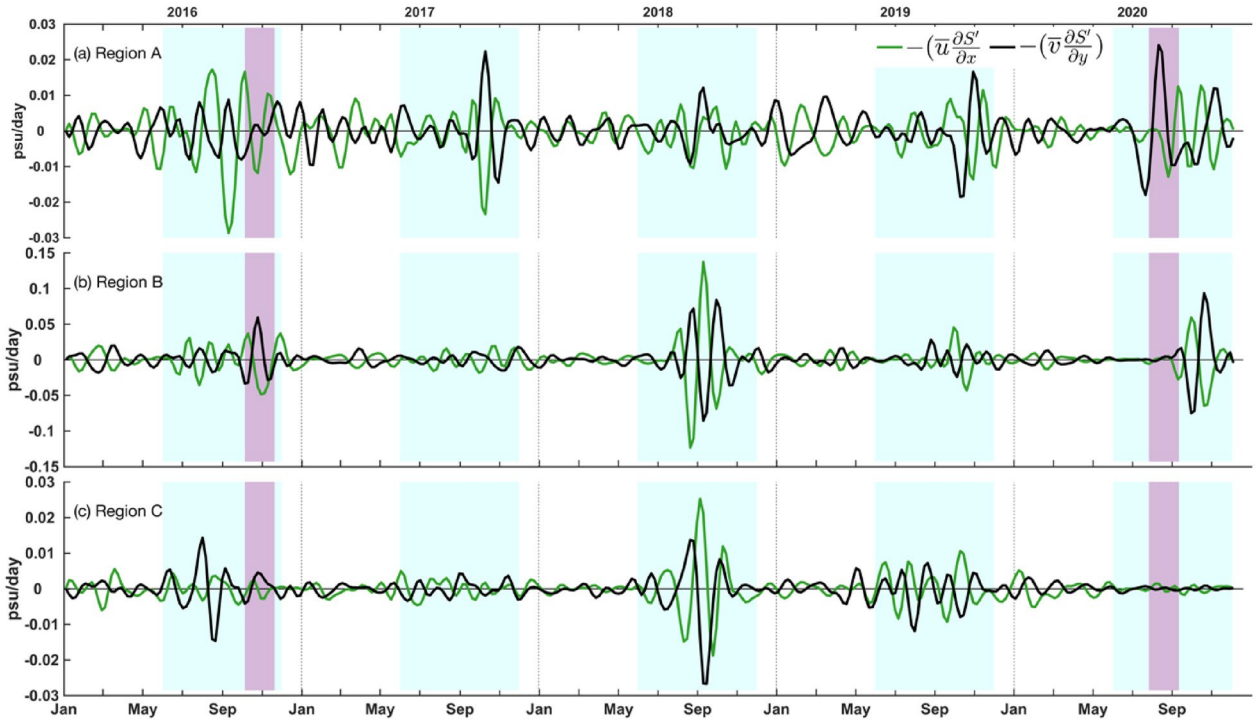

Fig. 12 Time series of anomalous advection by the mean zonal current advecting anomalous salinity (green, psu/day) and salinity transport by the mean meridional current advecting anomalous salinity (black, psu/day) for Region A, Region B and Region C during 2016–2020 from SODA data, respectively

There are potential interactions between anomalous perturbations in currents and freshwater inputs. The anomalous perturbations in the currents happen to overlap with the freshwater inputs and thus lead to a strengthening of the significant SSS ISV within the season. If the timing and direction of anomalous currents align with freshwater discharge, they might amplify the advection of low-salinity water masses, leading to more pronounced SSS variations. For example, anomalous currents, possibly induced by factors like MJO or MISO, can coincide with periods of enhanced freshwater discharge from rivers. The interplay between these factors could result in the advection of low-salinity water over the region.

Conclusions

Using SMAP satellite SSS data and SODA reanalysis SSS data, this study provides new insights into the mechanism of SSS variability over the northern BoB on intraseasonal timescales. The results indicate that SSS ISV in the northern BoB is heavily impacted by freshwater input and its transportation. Specifically, significant ISV occurs frequently in regions with large anomalous horizontal salinity gradient, mainly near the river mouth (Region A) and along the east coast of India (Region B). High amplitudes of SSS variability are phase-locked (July–November) when the river discharge is abundant. Salinity budget analyses indicate that horizontal advection component is

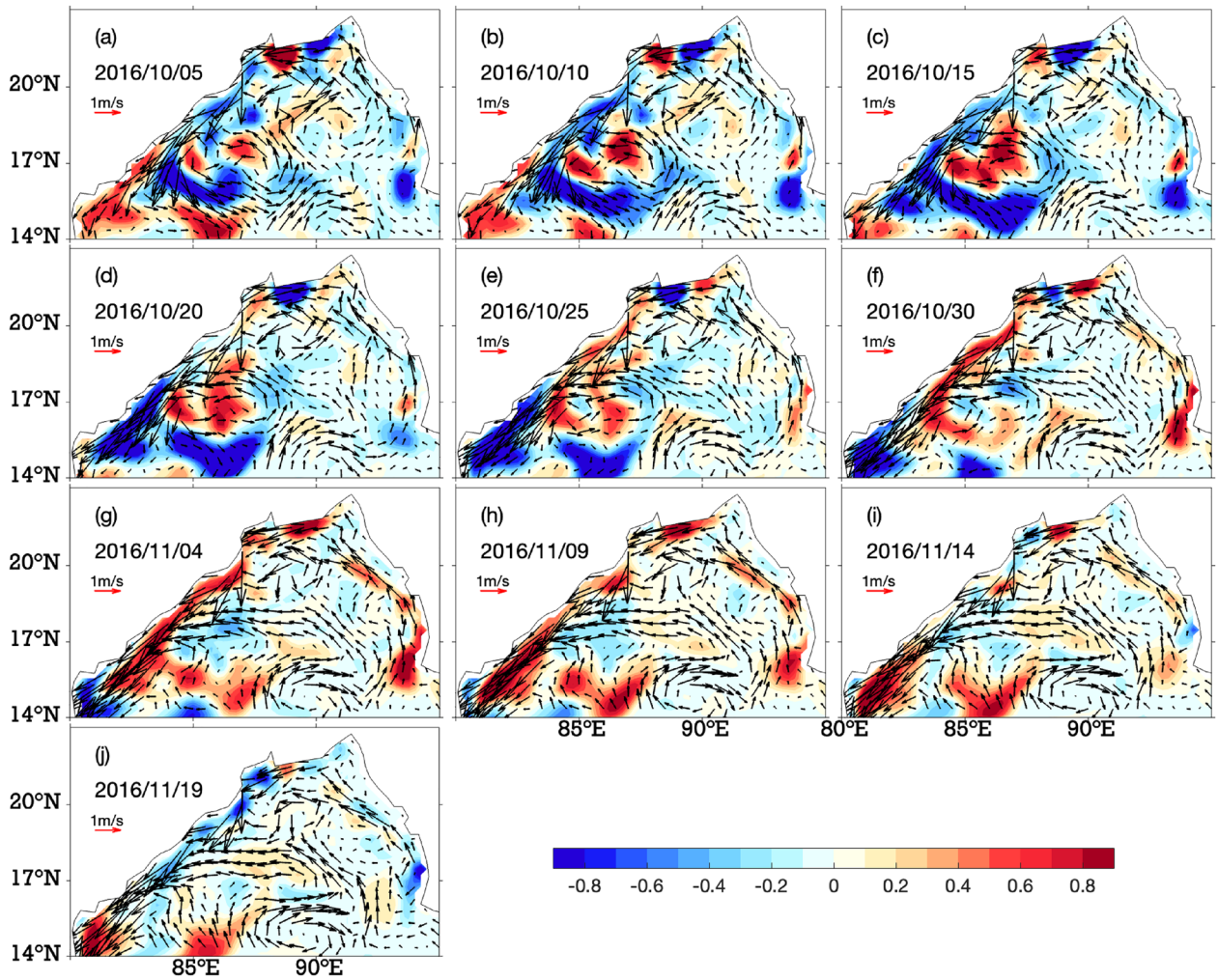

Fig. 13 The maps of 30–60-day SSS anomalies (unit: psu) and the mean surface current (arrows, unit: m/s) from SODA data during the period I

the leading driver of SSS ISV. The mean salinity advected by anomalous current (ADV1) and anomalous salinity advected by the mean current (ADV2) both play crucial roles. To further understand the processes that facilitate the anomalous advection, ADV1 and ADV2 during selected periods were examined.

In conclusion, this study broadens our understanding of the role of riverine freshwater and ocean dynamic processes in SSS ISV on intraseasonal timescales. These findings have important implications for ocean dynamics and air-sea interaction, particularly in the context of climate change. The study's limitations provide opportunities for future research to investigate the impact of SSS ISV on ocean dynamics, climate, and marine ecosystems in the northern BoB.

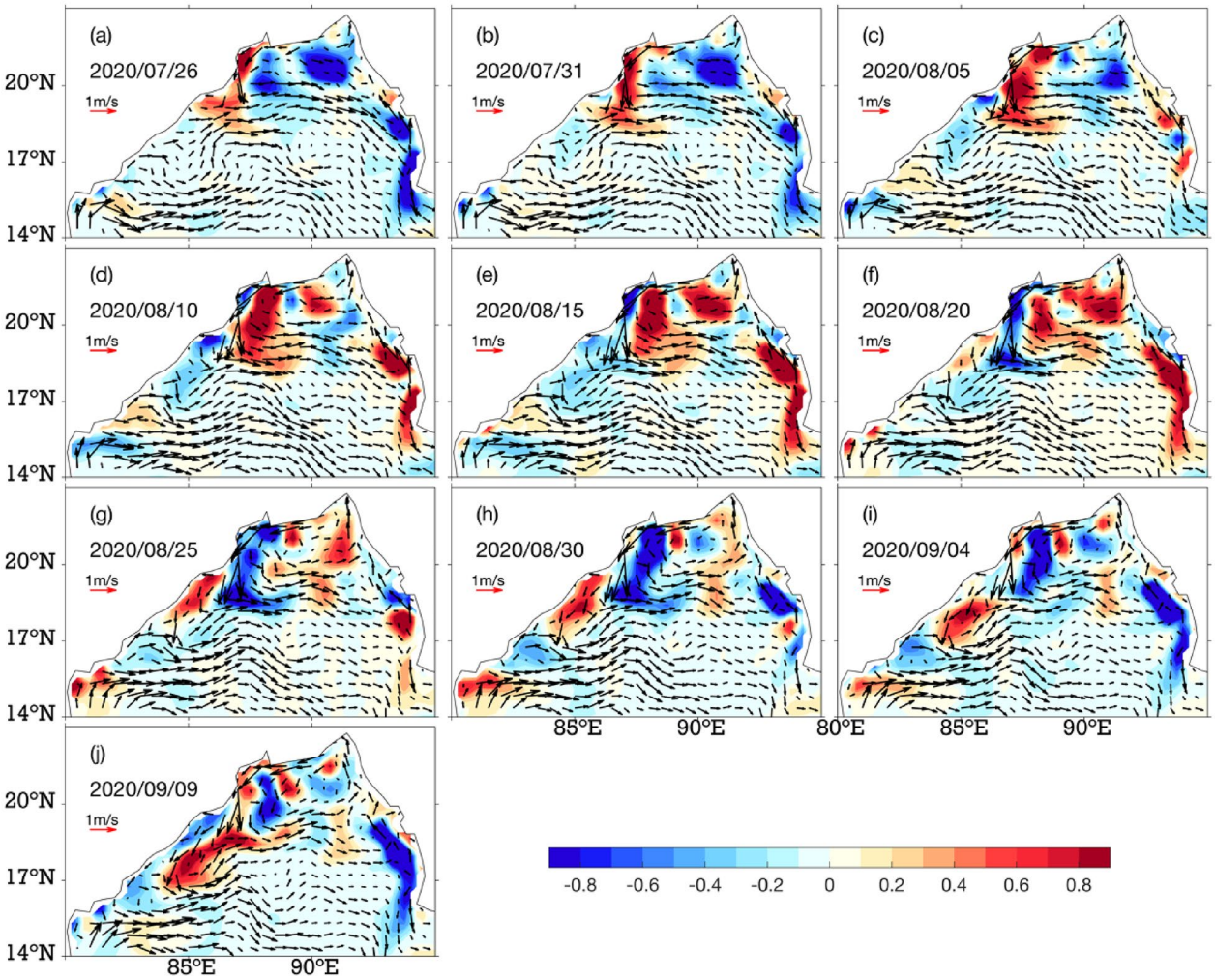

Fig. 14 The maps of 30–60-day SSS anomalies (unit: psu) and the mean surface current (arrows, unit: m/s) from SODA data during the period II

Author contributions
XC provided financial support for this study. RC carried out data analyses, and prepared for the manuscript. WD, LJ and YZ commented on earlier versions of the manuscript. All authors read and approved the final manuscript.

Funding
Xuhua Cheng is supported by the Natural Science Foundation of China (Grant 41876002, 42276014). Jianhuang Qin is supported by the National Natural Science Foundation of China (Grant 42106003).

Availability of data and materials
The SMAP data are downloaded from downloaded from NASA's Physical Oceanography Distributed Active Archive Center, and the SSS product was downloaded from the website: (https://podaac.jpl.nasa.gov/dataset/SMAP_JPL_L3_SSS_CAP_MONTHLY_V43?ids=&values=). SODA data are available on the website (http://dsrs.atmos.umd.edu/DATA/soda3.15.2/ORIGINAL/ocean/).

Declarations

Competing interests
The authors declare that they have no competing interests.

Received: 12 November 2023 Accepted: 20 March 2024
Published online: 18 April 2024

References

Akhil VP, Durand F, Lengaigne M, Vialard J, Keerthi MG, Gopalakrishna VV, Deltel C, Papa F, de Boyer MC (2014) A modeling study of the processes of surface salinity seasonal cycle in the Bay of Bengal. J Geophys Res 119:3926–3947. https://doi.org/10.1002/2013JC009632

Balaguru K, Chang P, Saravanan R, Leung L R, Xu Z, Li M, Hsieh J-S (2012) Ocean barrier layers' effect on tropical cyclone intensification. PNAS 109(36):14343–14347. https://doi.org/10.1073/pnas.1201364109

Bao S, Wang H, Zhang R, Yan H, Chen J (2019) Comparison of satellite-derived sea surface salinity products from SMOS, Aquarius, and SMAP. J Geophys Res. https://doi.org/10.1029/2019JC014937

Benshila R, Durand F, Masson S, Bourdalle-Badie R, de Boyer MC, Papa F, Madec G (2014) The upper Bay of Bengal salinity structure in a high-resolution model. Ocean Model 74:36–52. https://doi.org/10.1016/j.ocemod.2013.12.001

Carton JA, Chepurin GA, Chen L (2018) SODA3: a new ocean climate reanalysis. J Clim 31:6967–6983. https://doi.org/10.1175/JCLI-D-18-0149.1
Chaitanya AVS, Durand F, Mathew S, Gopalakrishna VV, Papa F, Lengaigne M, Vialard M, Kranthikumar C, Venkatesan R (2015) Observed year-to-year sea surface salinity variability in the Bay of Bengal during the 2009–2014 period. Ocean Dyn 65:173–186. https://doi.org/10.1007/s10236-014-0802-x
Durand F, Shankar D, Birol F, Shenoi SSC (2009) Spatiotemporal structure of the East India Coastal Current from satellite altimetry. J Geophys Res 114:C02013. https://doi.org/10.1029/2008JC004807
Durand F, Papa F, Rahman A, Bala SK (2011) Impact of Ganges-Brahmaputra interannual discharge variations on Bay of Bengal salinity. J Earth Syst Sci 120(5):859–872. https://doi.org/10.1007/s12040-011-0118-x
Fournier S, Vialard J, Lengaigne M, Lee T, Gierach MM, Chaitanya AVS (2017) Modulation of the Ganges-Brahmaputra river plume by the Indian Ocean Dipole and eddies inferred from satellite observations. J Geophys Res 122(12):9591–9604. https://doi.org/10.1002/2017JC013333
Fujinami H, Hatsuzuka D, Yasunari T, Hayashi T, Terao T, Murata F (2011) Characteristic intraseasonal oscillation of rainfall and its effect on interannual variability over Bangladesh during boreal summer. Int J Climatol 31(8):1192–1204. https://doi.org/10.1002/joc.2146
Grunseich G, Subrahmanyam B, Arguez A (2011) Influence of the Madden-Julian Oscillation on sea surface salinity in the Indian Ocean. Geophys Res Lett 38:L17605. https://doi.org/10.1029/2011GL049047
Grunseich G, Subrahmanyam B, Wang B (2013) The Madden-Julian oscillation detected in Aquarius salinity observations. Geophys Res Lett 40(20):5461–5466. https://doi.org/10.1002/2013gl058173
Guan B, Lee T, Halkides DJ, Waliser DE (2014) Aquarius surface salinity and the Madden-Julian Oscillation: the role of salinity in surface layer density and potential energy. Geophys Res Lett 41:2858–2869. https://doi.org/10.1002/2014GL059704
Han W, McCreary JP (2001) Modeling salinity distribution in the Indian Ocean. J Geophys Res 106:859–877. https://doi.org/10.1029/2000JC000316
Han W, McCreary JP, Kohler KE (2001) Influence of precipitation minus evaporation and Bay of Bengal rivers on dynamics, thermo-dynamics, and mixed layer physics in the upper Indian Ocean. J Geophys Res 106:6895–6916. https://doi.org/10.1029/2000JC000403
Howden SD, Murtugudde R (2001) Effects of river inputs into the Bay of Bengal. J Geophys Res 19(106):825–843. https://doi.org/10.1029/2000JC000656
Kikuchi K, Wang B (2009) Global perspective of the quasi-biweekly oscillation. J Clim 22(6):1340–1359. https://doi.org/10.1175/2008JCLI2368.1
Krishnan R, Ayantika D C, Kumar V Pokhrel S (2011) The long-lived monsoon depressions of 2006 and their linkage with the Indian Ocean Dipole. Int J Climatol. 31: 1334–1352. https://doi.org/10.1002/joc.2156
Li K, Yu W, Li T, Murty VSN, Khokiattiwong S, Adi TR (2003) Structures and mechanisms of the first-branch northward propagating intraseasonal oscillation over the tropical Indian Ocean. Clim Dyn 40(7–8):1707–1720. https://doi.org/10.1007/s00382-012-1492-z
Li Y, Han W, Lee T (2015) Intraseasonal sea surface salinity variability in the equatorial Indo-Pacific Ocean induced by Madden-Julian Oscillations. J Geophys Res 120(3):2233–2258. https://doi.org/10.1002/2014JC010647
Li Y, Han W, Wang W, Ravichandran M, Shinoda T (2017a) Bay of Bengal salinity stratification and Indian summer monsoon intraseasonal oscillation: 1. Intraseasonal variability and causes. J Geophys Res 122(5):4291–4311. https://doi.org/10.1002/2017JC012691
Li Y, Han W, Wang W, Ravichandran M, Shinoda T (2017b) Bay of Bengal salinity stratification and Indian summer monsoon intraseasonal oscillation: 2. Impact on SST and convection. J Geophys Res 122:4312–4328. https://doi.org/10.1002/2017JC012692
Lukas R, Lindstrom E (1991) The mixed layer of the western equatorial Pacific Ocean. J Geophys Res 96:3343–3357. https://doi.org/10.1029/90JC01951
Madden RA, Julian PR (1971) Detection of a 40–50day oscillation in the zonal wind in the tropical Pacific. J Atmos Sci 28(5):702–708. https://doi.org/10.1175/1520-0469(1971)028<0702:DOADOI>2.0.CO;2
Madden RA, Julian PR (1972) Description of global-scale circulation cells in the tropics with a 40–50day period. J Atmos Sci 29(6):1109–1123. https://doi.org/10.1175/1520-0469(1972)029%3c1109:DOGSCC%3e2.0.CO;2
Mignot JC, de Mont B, Lazar A, Cravatte S (2007) Control of salinity on the mixed layer depth in the world ocean: 2. Tropical areas. J Geophys Res 112:C10010. https://doi.org/10.1029/2006JC003954
Narvekar J, Kumar SP (2006) Seasonal variability of the mixed layer in the central Bay of Bengal and associated changes in nutrients and chlorophyll. Deep-Sea Res Pt I 53:820–835. https://doi.org/10.1016/j.dsr.2006.01.012
Neetu S, Lengaigne M, Vincent EM, Vialard J, Madec G, Samson G, Ramesh Kumar MR, Durand F (2012) Influence of upper-ocean stratification on tropical cyclone-induced surface cooling in the Bay of Bengal. J Geophys Res 117:C12020. https://doi.org/10.1029/2012JC008433
Nyadjro ES, Subrahmanyam B, Murty VSN, Shriver JF (2012) The role of salinity on the dynamics of the Arabian Sea mini warm pool. J Geophys Res. https://doi.org/10.1029/2012jc007978
Pant V, Girishkumar MS, Udaya Bhaskar TVS, Ravichandran M, Papa F, Thangaprakash VP (2015) Observed interannual variability of near-surface salinity in the Bay of Bengal. J Geophys Res 120:3315–3329. https://doi.org/10.1002/2014JC010340
Papa F, Durand F, Rahman A, Bala SK, Rossow WB (2010) Satellite altimeter-derived monthly discharge of the Ganga-rahmaputra River and its seasonal to interannual variations from 1993 to 2008. J Geophys Res 115:C12013. https://doi.org/10.1029/2009JC006075
Parampil SR, Gera A, Ravichandran M, Sengupta D (2010) Intraseasonal response of mixed layer temperature and salinity in the Bay of Bengal to heat and freshwater flux. J Geophys Res 115(C5):C05002. https://doi.org/10.1029/2009JC005790
Rao RR, Sivakumar R (2003) Seasonal variability of sea surface salinity and salt budget of the mixed layer of the north Indian Ocean. J Geophys Res 108(C1):3009. https://doi.org/10.1029/2001JC00907
Rao SA, Durairaju RM, Girishkumar M, Ravichandran M (2020) Interannual variability of Bay of Bengal salinity: role of ocean and atmospheric dynamics. J Geophys Res 125(7):e2019JC015864
Sandeep KK, Pant V, Girishkumar MS, Rao AD (2017) Impact of riverine freshwater forcing on the sea surface salinity simulations in the Indian Ocean. J Mar Syst 185:40–58. https://doi.org/10.1016/j.jmarsys.2018.05.002
Schott F, McCreary JP (2001) The monsoon circulation of the Indian Ocean. Prog Oceanogr 51:1–123. https://doi.org/10.1016/S0079-6611(01)00083-0
Schott FA, Xie SP, McCreary JP (2009) Indian Ocean circulation and climate variability. Rev Geophys 47(1):RG1002. https://doi.org/10.1029/2007RG000245
Sengupta D, Bharath Raj GN, Shenoi SSC (2006) Surface freshwater from Bay of Bengal runoff and Indonesian throughflow in the tropical Indian Ocean. Geophys Res Lett 33(22):L22609. https://doi.org/10.1029/2006GL027573
Sengupta D, Bharath Raj RG, Anitha DS (2008) Cyclone-induced mixing does not cool SST in the post-monsoon north Bay of Bengal. Atmos Sci Lett 9:1–6. https://doi.org/10.1002/asl.162
Seo H, Xie SP, Murtugudde R, Jochum M, Miller AJ (2009) Seasonal effects of Indian Ocean freshwater forcing in a regional coupled model. J Clim 22:6577–6596. https://doi.org/10.1175/2009JCLI2990.1
Shankar D, McCreary JP, Han W, Shetye SR (1996) Dynamics of the East India Coastal Current 1. Analytic solutions forced by interior Ekman pumping and local alongshore winds. J Geophys Res 13(101):975–991. https://doi.org/10.1029/96JC00559
Shankar D, Vinayachandran PN, Unnikrishnan AS (2002) The monsoon currents in the north Indian Ocean. Prog Oceanogr 52:63–120. https://doi.org/10.1016/S0079-6611(02)00024-1
Sharma R, Agarwal N, Momin IM, Basu S, Agarwal VK (2010) Simulated sea surface salinity variability in the tropical Indian Ocean. J Clim 23:6542–6554. https://doi.org/10.1175/2010JCLI3721.1
Shenoi SSC, Shankar D, Shetye SR (2002) Difference in heat budgets of the near-surface Arabian Sea and Bay of Bengal: implications for the summer monsoon. J Geophys Res 107(C6):3052. https://doi.org/10.1029/2000JC000679
Shenoi SSC, Shankar D, Michael GS, Kurian J, Varma KK, Ramesh Kumar MR, Almeida Unnikrishnan AS, Fernandes W, Barreto N, Gnanaseelan C, Mathew R, Praju KV, Mahale V (2005) Hydrography and water masses in the southeastern Arabian Sea during March–June 2003. J Earth Syst Sci 114:475–491. https://doi.org/10.1007/BF02702024
Subrahmanyam B, Trott CB, Murty VSN (2018) Detection of Intraseasonal Oscillations in SMAP salinity in the Bay of Bengal. Geophys Res Lett 45(14):7057–7065. https://doi.org/10.1029/2018GL078662
Tang W, Fore A, Yueh S, Lee T, Hayashi A, Sanchez-Franks A, King B, Baranowski D (2017) Validating SMAP SSS with in-situ measurements. Remote Sens Environ 200:326–340. https://doi.org/10.1016/j.rse.2017.08.021

Trott CB, Subrahmanyam B, Roman-Stork HL, Murty VSN, Gnanaseel C (2019) Variability of intraseasonal oscillations and synoptic signals in sea surface salinity in the Bay of Bengal. J Clim 20(32):6703–6728. https://doi.org/10.1175/JCLI-D-19-0178.1

Vinayachandran PN, Kurian J (2007) Hydrographic observations and model simulation of the Bay of Bengal freshwater plume. Deep Sea Res 54:471–486. https://doi.org/10.1016/j.dsr.2007.01.007

Vinayachandran P N, Murty V S N, Ramesh Babu V (2002) Observations of barrier layer formation in the Bay of Bengal during summer monsoon. J Geophys Res 107:8018. https://doi.org/10.1029/2001JC000831..

Vinayachandran PN, Nanjundiah RS (2009) Indian Ocean sea surface salinity variations in a coupled model. Clim Dyn 33:245–263. https://doi.org/10.1007/s00382-008-0511-6

Vinayachandran PN, Murty VSN, Ramesh Babu V (2001) Observations of barrier layer formation in the Bay of Bengal during summer monsoon. J Geophys Res 107(C12):8018. https://doi.org/10.1029/2001JC000831

Vinayachandran PN, Neema CP, Mathew S, Remya R (2012) Mechanisms of summer intraseasonal sea surface temperature oscillations in the Bay of Bengal. J Geophys Res 117:C01005. https://doi.org/10.1029/2011JC007433

Vinayachandran PN, Shankar D, Vernekar S, Sandeep KK, Amol P, Neema CP, Chatterjee A (2013) A summer monsoon pump to keep the Bay of Bengal salty. Geophys Res Lett 40:1777–1782. https://doi.org/10.1002/grl.50274

Vincent EM, Lengaigne M, Vialard J, Madec G, Jourdain N, Masson S (2012) Assessing the oceanic control on the amplitude of sea surface cooling induced by tropical cyclones. J Geophys Res 117:C05023. https://doi.org/10.1029/2011JC007705

Vinogradova N, Lee T, Boutin J, Drushka K, Fournier S, Sabia R, Melnichenko O (2019) Satellite salinity observing system: recent discoveries and the way forward. Front Mar Sci 6:243. https://doi.org/10.3389/fmars.2019.00243

Wang B, LinHo (2002) Rainy Season of the Asian–Pacific Summer Monsoon. J Clim 15(4):386–398. https://doi.org/10.1175/1520-0442(2002)0152.0.CO;2

Webster PJ et al (2002) The JASMINE Pilot Study. Bull Am Meteorol Soc 83:1603–1630. https://doi.org/10.1175/BAMS-83-11-1603

Wijesekera HW, Shroyer E, Tandon A, Ravichandran M, Sengupta D, Jinadasa SUP, Fernando HJ, Agrawal N, Arulananthan K, Bhat GS, Baumgartner M (2016) ASIRI: an ocean-atmosphere initiative for Bay of Bengal. Bull Am Meteorol Soc 97(10):1859–1884. https://doi.org/10.1175/BAMS-D-14-00197.1

Wu L, Wang F, Yuan D, Cui M (2007) Evolution of freshwater plumes and salinity fronts in the northern Bay of Bengal. J Geophys Res 112:C08017. https://doi.org/10.1029/2005JC003308

Yu Z, McCreary JP (2004) Assessing precipitation products in the Indian Ocean using an ocean model. J Geophys Res 109:C05013. https://doi.org/10.1029/2003JC002106

Zhu J, Kumar A, Wang W (2020) Intraseasonal surface salinity variability and the MJO in a climate model. Geophys Res Lett 47:e2020GL088997. https://doi.org/10.1029/2020GL088997

Zhang Y, Xu H, Du Y, Wang D (2009) Seasonal variability of salinity budget in the southeastern Arabian Sea. J Trop Oceanogr 2009(5): 66 –74. https://doi.org/10.11978/j.issn.1009-5470.2009.05.066

Publisher's Note